

Universal scaling laws for correlation spreading in quantum systems with short- and long-range interactions

Lorenzo Cevolani,¹ Julien Despres,² Giuseppe Carleo,^{3,4} Luca Tagliacozzo,⁵ and Laurent Sanchez-Palencia²

¹*Institut für Theoretische Physik, Georg-August-Universität Göttingen, 37077 Göttingen, Germany*

²*Centre de Physique Théorique, Ecole Polytechnique, CNRS, Université Paris-Saclay, F-91128 Palaiseau, France*

³*Institute for Theoretical Physics, ETH Zurich, Wolfgang-Pauli-Strasse 27, 8093 Zurich, Switzerland*

⁴*Center for Computational Quantum Physics, Flatiron Institute, 162 5th Avenue, New York, New York 10010, USA*

⁵*Department of Physics and SUPA, University of Strathclyde, Glasgow G4 0NG, United Kingdom*



(Received 8 June 2017; revised manuscript received 20 June 2018; published 5 July 2018)

The spreading of correlations after a quantum quench is studied in a wide class of lattice systems, with short- and long-range interactions. Using a unifying quasiparticle framework, we unveil a rich structure of the correlation cone, which encodes the footprints of several microscopic properties of the system. When the quasiparticle excitations propagate with a bounded group velocity, we show that the correlation edge and correlation maxima move with different velocities that we derive. For systems with a divergent group velocity, especially relevant for long-range interacting systems, the correlation edge propagates slower than ballistic. In contrast, the correlation maxima propagate faster than ballistic in gapless systems but ballistic in gapped systems. Our results shed light on existing experimental and numerical observations and pave the way to the next generation of experiments. For instance, we argue that the dynamics of correlation maxima can be used as a witness of the elementary excitations of the system.

DOI: [10.1103/PhysRevB.98.024302](https://doi.org/10.1103/PhysRevB.98.024302)

I. INTRODUCTION

The ability of a quantum system to establish long-distance correlations and entanglement, and possibly equilibrate, is determined by the speed at which information can propagate within the system. For lattice models with short-range interactions, Lieb and Robinson (LR) have unveiled a bound that forms a linear causality cone beyond which information decays exponentially [1]. This bound implies ballistic propagation of equal time-correlation functions [2] that has been observed experimentally [3,4] and characterized numerically [5–9]. Generalized LR bounds have been derived for long-range systems where the interactions decay algebraically, $1/R^\alpha$, with the distance R (see Refs. [10,11]). The related experiments and numerical investigations have, however, led to conflicting pictures [12–18]. For instance, experiments on ion chains [15] and numerical simulations within the truncated Wigner approximation [19] for the one-dimensional (1D) long-range XY (LRXY) model point towards bounded, superballistic propagation for all values of α . In contrast, experiments on the long-range transverse Ising (LRTI) model reported ballistic propagation of correlation maxima with, however, observable leaks that increase when α decreases [14]. Moreover, time-dependent density-matrix renormalization group (t-DMRG) and variational Monte Carlo (t-VMC) numerical simulations indicate the existence of three distinct regimes, namely, instantaneous, subballistic, and ballistic, for increasing values of the exponent α (see Refs. [12,13,16–18,20]).

In this paper we shed light on these apparent contradictions. We focus on equal-time correlation functions that are relevant experimentally. Implications of bounded correlation spreading on universal LR bounds are not yet completely understood (see,

however, Ref. [21]), so we do not draw explicit conclusions on the latter.

Using a universal picture based on quasiparticles that can be applied to both short- and long-range models, we unveil a double causality structure for correlation spreading. The *outer structure* determines the correlation edge (CE), while the *inner structure* determines the propagation of local extrema. For short-range interactions, the two structures are determined by the dispersion relation and can be associated with, respectively, the group and phase velocities of the quasiparticles. For long-range interactions, the inner structure is still determined by the dispersion relation. It is superballistic for gapless models and ballistic for gapped models. It implies that quantum quenches can be used experimentally as a witness to detect the presence of the gap and the value of the dynamical exponent of the underlying model, something that as far as we know was not realized previously. The outer structure depends both on the dispersion relation and on the considered observable and is thus less universal. Except in pathologic cases, it is always subballistic.

The identification of this double structure (i.e., edge versus local maxima of correlations) and the lack of universality of the outer edge in long-range systems permit us to accommodate and explain previous observations in a unified picture. This result is particularly important result to predict the spreading of specific observables and design the next generation of experiments within a large class of long-range systems, e.g., Rydberg gases [22–25], nonlinear optical media [26], polar molecules [27–29], magnetic atoms [30–34], superconductors [35], ion chains [36–40], and solid-state defects [41–43].

II. TIME EVOLUTION OF LOCAL CORRELATIONS

Consider a quantum system defined on a hypercubic lattice of dimension D and governed by a translation-invariant Hamiltonian of the form

$$\hat{H} = \sum_{\mathbf{R}} h(\mathbf{R}) \hat{K}_1(\mathbf{R}) + \sum_{\mathbf{R}, \mathbf{R}'} J(\mathbf{R}, \mathbf{R}') \hat{K}_2(\mathbf{R}, \mathbf{R}'), \quad (1)$$

where \mathbf{R} and \mathbf{R}' span the lattice sites. The first term accounts for local interactions, and the second term accounts for two-site couplings. It applies to a variety of models, including the Bose-Hubbard (BH; see Appendix A), the LRXY, and the LRTI (see Appendix B), which we consider in the following. We start from the ground state of \hat{H} and quench the system out of equilibrium by changing the couplings at time $t = 0$. We characterize the evolution by computing equal-time connected correlation functions with respect to the pre-quench equilibrium value. They read $G(\mathbf{R}, t) \equiv G_0(\mathbf{R}, t) - G_0(\mathbf{R}, 0)$, with $G_0(\mathbf{R}, t) \equiv \langle \hat{A}_X(t) \hat{B}_Y(t) \rangle - \langle \hat{A}_X(t) \rangle \langle \hat{B}_Y(t) \rangle$, where \hat{A}_X and \hat{B}_Y are local operators with support in regions X and Y separated by \mathbf{R} . Such correlations can be measured in state-of-the-art experiments [3,4,14,15]. We describe quenches where the dynamics is driven by the low-energy sector of \hat{H} that may be assumed to consist of quasiparticle excitations. Due to translation invariance, they are characterized by well-defined quasimomentum \mathbf{k} and energy $E_{\mathbf{k}}$. The correlation functions may be written

$$G(\mathbf{R}, t) = g(\mathbf{R}) - \int_{\mathcal{B}} \frac{d\mathbf{k}}{(2\pi)^D} \mathcal{F}(\mathbf{k}) \times \frac{e^{i(\mathbf{k} \cdot \mathbf{R} + 2E_{\mathbf{k}}t)} + e^{i(\mathbf{k} \cdot \mathbf{R} - 2E_{\mathbf{k}}t)}}{2}, \quad (2)$$

where the integral spans the first Brillouin zone \mathcal{B} . The quantity $g(\mathbf{R})$ can be dropped since it does not depend on time. Equation (2) represents the motion of counterpropagating quasiparticle pairs, with velocities determined by $E_{\mathbf{k}}$, where the amplitude $\mathcal{F}(\mathbf{k})$ encodes the overlap of the initial state with the quasiparticle wave functions and the matrix elements of \hat{A} and \hat{B} . It can be derived explicitly in exactly solvable models and quadratic systems, which can be diagonalized by means of canonical transformations. Many models, in various regimes, can be mapped into this form (see, for instance, Refs. [6,12,16–18,44,45] in the context of out-of-equilibrium dynamics). The concept of quasiparticles also applies to models that are not exactly solvable, where they can be determined using tensor-network techniques [46,47], for instance, and we expect that our results also hold for such systems.

III. SHORT-RANGE COUPLINGS

Consider first the case of nearest-neighbor interactions for which the quasiparticle group velocity is bounded. In the infinite-time and -distance limit along the line $R/t = \text{const}$, the integral in Eq. (2) is dominated by the momentum contributions with a stationary phase (sp), i.e., $\nabla_{\mathbf{k}}(kR \mp 2E_{\mathbf{k}}t) = 0$ or, equivalently,

$$2V_{\mathbf{g}}(k_{\text{sp}}) = \pm R/t, \quad (3)$$

where $V_{\mathbf{g}} = \nabla_{\mathbf{k}} E_{\mathbf{k}}$ is the group velocity. Since the latter is upper bounded by some value $V_{\mathbf{g}}^*$, Eq. (3) has a solution only for

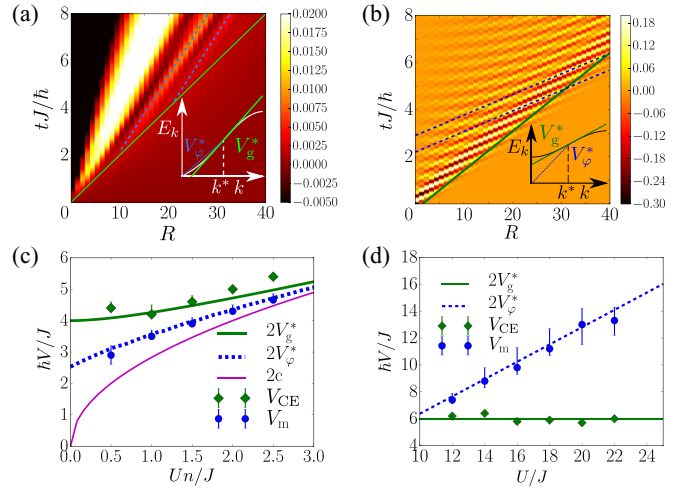


FIG. 1. Top: Spreading of the connected one-body correlation function $G(R, t) = \langle \hat{a}_k^\dagger(t) \hat{a}_0(t) \rangle - \langle \hat{a}_k^\dagger(0) \hat{a}_0(0) \rangle$ for the 1D Bose-Hubbard model. (a) Superfluid phase for a quench from the initial value $U_i n = J$ to the final value $U_f n = 0.5J$. (b) Mott-insulator phase with $n = 1$ for a quench from $U_i = \infty$ to $U_f = 18J$. The solid green and dashed blue lines indicate ballistic spreading at twice the maximum group velocity $2V_{\mathbf{g}}^*$ and twice the corresponding phase velocity $2V_{\phi}^*$, respectively. Bottom: Comparison between the maximum group velocity $V_{\mathbf{g}}^*$ (solid green line), the corresponding phase velocity V_{ϕ}^* (dashed blue line), the sound velocity c (solid purple line), and fits to the LR cone velocity V_{CE} (green diamonds) and to the velocity of the maxima V_{m} (blue disks) for the (c) superfluid and (d) Mott insulator phases with the same initial values as for (a) and (b).

$R/t < 2V_{\mathbf{g}}^*$. The correlation function then reads [48]

$$G(R, t) \propto \frac{\mathcal{F}(k_{\text{sp}})}{(|\nabla_{\mathbf{k}}^2 E_{k_{\text{sp}}}|t)^{\frac{D}{2}}} \cos\left(k_{\text{sp}}R - 2E_{k_{\text{sp}}}t + \frac{\pi}{4}\right). \quad (4)$$

For $R/t > 2V_{\mathbf{g}}^*$, Eq. (3) has no solution, and $G(R, t)$ is vanishingly small. The correlations are thus activated ballistically at the time $t = R/2V_{\mathbf{g}}^*$. This formula defines a linear correlation edge (CE) with velocity $V_{\text{CE}} = 2V_{\mathbf{g}}^*$, consistent with the Calabrese-Cardy picture [49].

Yet Eq. (4) yields not only the CE but also a series of local maxima. In the vicinity of the CE cone, only the quasiparticles with momenta $k \simeq k^*$, which move at $V_{\mathbf{g}}^*$, contribute to the correlations. There the maxima (m), defined by the equation $k^*R - 2E_{k^*}t = \text{const}$, propagate at the velocity $V_{\text{m}} = 2V_{\phi}^* \equiv 2E_{k^*}/k^*$, i.e., twice the phase velocity at the maximum of the group velocity k^* . Since the phase and group velocities are generally different, the CE is expected to feature a double structure characterized by these two velocities. This observation and its counterpart for long-range systems (see below) have fundamental consequences for correlation spreading and are the pivotal result of this work.

To illustrate, let us consider the BH model. In the superfluid regime, the dispersion relation is bounded, and the group velocity has a local maximum at some momentum $0 < k^* < \pi$ [see the inset in Fig. 1(a)]. The main panel of Fig. 1(a) shows the connected one-body correlation function versus distance and time in this regime. Its value is determined

from numerical integration of Eq. (2) with the coefficients calculated using Bogoliubov theory. The latter holds for weak interactions, $Jn \gg U$, with J being the hopping and U being the interaction strength (see Appendix A for details). As expected, the correlation cone is determined by the velocity $V_{\text{CE}} \simeq 2V_{\text{g}}^*$ (solid green line). Moreover, the correlations show a series of local maxima, all propagating at the same speed, approximately twice the phase velocity at the momentum k^* , $V_{\text{m}} \simeq 2V_{\varphi}^*$ (dashed blue lines). These observations are confirmed quantitatively in Fig. 1(c), where we compare the values of the velocities found from fits to the correlation edge (V_{CE}) and local maxima (V_{m}), on the one hand, to twice the group (V_{g}^*) and phase (V_{φ}^*) velocities at k^* , on the other hand.

The distinction between the edge propagating at V_{g}^* and the maxima emanating from it and propagating at V_{φ}^* permits us to understand previously unexplained observations. The propagation velocity extracted from t-VMC calculations in Ref. [7] quantitatively agrees with the value $2V_{\varphi}^*$ calculated here. Our analysis shows that it should thus be assimilated to the propagation of the local maxima, i.e., the inner structure of the causal region [50]. In contrast, the CE is determined by the increase of the envelop of these maxima and moves at the velocity $2V_{\text{g}}^*$. The same analysis applies to the results of t-DMRG calculations for a quench in the superfluid regime of the Fermi-Hubbard model [5].

So far experimental characterization of correlation spreading for a quench in the Mott-insulator regime has been performed close to the critical point where there is a single characteristic velocity, and as a consequence, no inner structure has been observed [3]. A richer behavior occurs deeper in the Mott regime, where the presence of a gap permits us to find a regime, $U > \pi(2n+1)J$, where $V_{\varphi}^* > V_{\text{g}}^*$ [see the inset in Fig. 1(b)]. Here the excitation spectrum is found using strong-coupling perturbation theory, which holds for $n \in \mathbb{N}^*$ and $U \gg Jn$ (see Appendix A). The connected one-body correlation function plotted in Fig. 1(b) is found from numerical integration of Eq. (2) with the corresponding coefficients. In this case, the local maxima propagate (still at V_{φ}^*) faster than the correlation cone (still at V_{g}^*) and vanish when reaching it [see Figs. 1(b) and 1(d)].

IV. LONG-RANGE COUPLINGS

We now turn to long-range systems with power-law couplings, $J_{\mathbf{R},\mathbf{R}'} \sim J/|\mathbf{R}-\mathbf{R}'|^\alpha$. We assume that the spectrum is regular in the whole Brillouin zone, except for a cusp at $k=0$. There, the dispersion relation may be written $E_k \simeq \Delta + ck^z$, with z being the dynamical exponent and Δ being the (possibly vanishing) gap. For $0 < z < 1$ the quasiparticle energy E_k is bounded, but the group velocity $V_{\text{g}}(k)$ diverges. In the following, we consider connected spin correlation functions for two spin models, as found from Eq. (2) and linear spin-wave theory (see Appendix B and references therein). All quenches are performed in a single polarized phase, without crossing any critical line.

Figure 2(a) corresponds to the LRXY model. Owing to continuous spin-rotation symmetry, it is gapless, $\Delta = 0$, and $z = (\alpha - D)/2$ for $D < \alpha < D + 2$ (see Ref. [51]). Figure 2(b) corresponds to the LRTI model, where the transverse magnetic field opens a gap, $\Delta > 0$, and $z = \alpha - D$ for

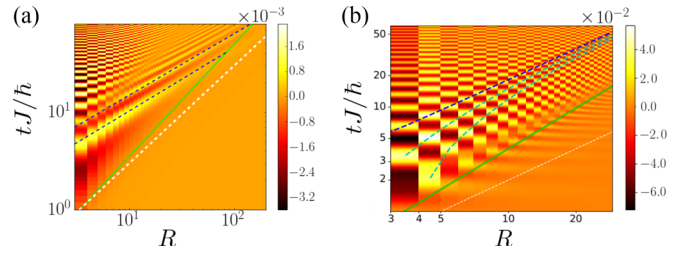


FIG. 2. Spreading of the connected spin correlation function $G(R,t) = G_0(R,t) - G_0(R,0)$ for the following 1D models: (a) LRXY model with $\alpha = 2.3$, $G_0(R,t) = \langle S_R^z(t)S_0^z(t) \rangle - \langle S_R^z(t) \rangle \langle S_0^z(t) \rangle$ for a quench from the ground state of the XXZ model ($\epsilon = 0.2$; see Appendix B) and (b) LRTI model with $\alpha = 1.7$, $G_0(R,t) = \langle S_R^x(t)S_0^x(t) \rangle - \langle S_R^x(t) \rangle \langle S_0^x(t) \rangle$ for the quench in the polarized phase from $J_i/h = 0.02$ to $J_t/h = 1$ (see Ref. [52]). They feature a double algebraic structure (straight lines in log-log scale): a subballistic correlation edge (solid green line) and superballistic or ballistic spreading of local maxima (dashed blue lines). The white dotted line indicates ballistic spreading for reference. The light blue dashed lines are guides to the eye.

$D < \alpha < D + 1$ (see Refs. [12,16,17]). For both models, we find a double structure reminiscent of the one of short-range models, although with crucial differences. First, the CE is not linear but algebraic (note the log-log scales in Fig. 2). While the known extended LR bounds [10,11] are all superballistic, we find a *subballistic* CE, $t \sim R^{\beta_{\text{CE}}}$, with $\beta_{\text{CE}} > 1$ (the edges are marked by solid green lines and, for reference, ballistic spreading is shown by white dotted lines). Second, the inner structure shows a strongly model dependent behavior: For the LRXY model [Fig. 2(a)], the correlation maxima (dashed blue lines) are *superballistic*, $t \sim R^{\beta_{\text{m}}}$, with $\beta_{\text{m}} < 1$, while for the LRTI model [Fig. 2(b)] they are *ballistic*, $t \sim R$.

To understand these behaviors, let us use again the stationary-phase approximation. Equations (3) and (4) still hold. However, the group velocity, $V_{\text{g}}(k) = |c|z/k^{1-z}$, now diverges at $k \rightarrow 0$. Hence, for any combination of t and R , there is a quasiparticle with the corresponding group velocity at the momentum $k_{\text{sp}} = (2|c|zt/R)^{1/(1-z)}$. The CE is thus dominated by the infrared divergence, where we now need to analyze the amplitude function \mathcal{F} . Inserting the assumed scaling $\mathcal{F}(k) \sim k^\nu$, with $\nu \geq 0$, into Eqs. (3) and (4), we find

$$G_{\text{c}}(R,t) \propto \frac{t^\gamma}{R^\chi} \cos \left[A_z \left(\frac{t}{Rz} \right)^{\frac{1}{1-z}} - 2\Delta t + \frac{\pi}{4} \right], \quad (5)$$

with $\gamma = \frac{\nu+D/2}{1-z}$, $\chi = \frac{\nu+D(2-z)/2}{1-z}$, and $A_z = 2|c|(1-z)(2|c|z)^{\frac{z}{1-z}}$. The CE is found by imposing that the amplitude of the correlation function becomes of order 1. It yields the algebraic form

$$t^* \propto R^{\beta_{\text{CE}}}, \quad \beta_{\text{CE}} = \chi/\gamma. \quad (6)$$

Hence, the scaling of the CE depends not only on the dynamical exponent z but also on the specific correlation function via the exponent ν and on the dimension D . This contrasts with the short-range case, where a ballistic propagation independent of the dimension and of the observable is found [53]. Since $\chi = \gamma + D/2$, the CE is always subballistic, $\beta_{\text{CE}} > 1$. For the LRXY model and spin-spin correlations, we have $\nu =$

$z = (\alpha - D)/2$, which yields $\beta_{\text{CE}} = 1 + \frac{D}{2\alpha}(2 + D - \alpha)$. In the numerical calculations of Fig. 2(a), the CE is found by tracing the points in the R - t plane, where the correlations reach $\epsilon = 2\%$ of the maximal value. The activation time t^* as a function of the distance R is then fitted by a power law, $t^* \sim R^{\beta_{\text{CE}}^{\text{fit}}}$ (see details in Appendix D). For $\alpha = 2.3$ and $D = 1$ [Fig. 2(a)], we find $\beta_{\text{CE}}^{\text{fit}} \simeq 1.083 \pm 0.013$, in good agreement with the theoretical value $\beta_{\text{CE}} \simeq 1.15$.

For the LRTI model, we have $z = \alpha - D$ and $\nu = 0$. It yields the exponent $\beta_{\text{CE}} = 2 - z = 2 + D - \alpha$ completely determined by the dynamical exponent z . For $\alpha = 1.7$ and $D = 1$ [Fig. 2(b)], analyzing the numerical results as before, we find the CE exponent $\beta_{\text{CE}}^{\text{fit}} = 1.28 \pm 0.02$, in excellent agreement with the theoretical value $\beta_{\text{CE}} = 1.3$. Note that the general formula for β_{CE} matches the exact result of Ref. [16] for $D = 1$ and $\alpha = 3/2$ (i.e., $z = 1/2$), also confirmed by t-VMC calculations, and it is in fair agreement with the analysis of Ref. [17] for the 1D and 2D LRTI models.

On the other hand, the inner structure of the causal region is determined by the local maxima of the cosine function in Eq. (5). It does not depend on the observable but on the presence or absence of a gap. For a gapless system ($\Delta = 0$), we find

$$t_m \propto R^{\beta_m}, \quad \beta_m = z. \quad (7)$$

The correlation maxima are thus always superballistic, $\beta_m < 1$. For the LRXY model and $\alpha = 2.3$ [Fig. 2(a)], we find the theoretical value $\beta_m = 0.65$. In the numerics, we study the internal structure of the correlation function by tracking the position of the first local maximum as a function of time. We then fit the corresponding function by $t_m = aR^{\beta_m^{\text{fit}}} + b$. For the parameters of Fig. 2(a), it yields $\beta_m^{\text{fit}} \simeq 0.634 \pm 0.014$, in excellent agreement with the theoretical value. It is also consistent with the experimental observation of superballistic dynamics in the 1D LRXY model realized with trapped ion chains for $\alpha > 1$ (see Ref. [15]) and in rough agreement with the analysis of numerical calculations performed within the truncated Wigner approximation for 1D and 2D LRXY models [19]. The same result as Eq. (7) was found in Ref. [45], which appeared recently. Our analysis shows that this superballistic behavior characterizes the inner structure but not the CE.

For a gapped system ($\Delta > 0$), the momentum dependence of the dispersion relation becomes irrelevant in the infrared limit, and the argument of the cosine function in Eq. (5) is constant in the large- t and $-R$ limit for $t \propto R$. It follows that the local maxima are here always ballistic, $\beta_m = 1$. This case applies to the LRTI model. It is confirmed in Fig. 2(b), where we observe that the local maxima converge to a ballistic propagation for sufficiently long times. Performing the analysis as above, we find $\beta_m^{\text{fit}} \simeq 1.0045 \pm 0.0003$, in excellent agreement with the theoretical prediction. This result is consistent with the observation of ballistic motion of local maxima for the 1D LRTI model realized with trapped-ion chains [14].

V. CONCLUSIONS

In this work we have shown that the spreading of equal-time correlations has a double structure whose scaling laws can be related to different characteristic spectral properties. For short-range systems, they are readily associated with the group

and phase velocities, which generally differ. For long-range systems with a diverging group velocity, the CE is observable dependent and subballistic. Close to the CE, the local maxima propagate ballistically in gapped systems and superballistically in gapless systems. Their observation can thus be used as an experimental footprint for the presence of a spectral gap.

This double structure can be observed experimentally. Our analysis provides just the first step of an important research problem that aims at unveiling the physical information encoded in correlation spreading and it this can be extracted in the next generation of experiments (see also [9] for recent results in this direction). In practice, the dynamics of the local maxima is easier to observe, and as discussed above, our predictions are consistent with existing observations. Our analysis shows, however, that in generic experiments characterizing the spreading of correlations the data need to be interpreted very carefully. The propagation of local extrema does not characterize the correlation edge. Identifying the latter requires an accurate scaling analysis of the leaks. Existing experimental data have been collected either in a regime of parameters where the two structures coincide [3] or in small systems where quantitative analysis is obfuscated by strong finite-size effects. However, the next generation of experiments based on Rydberg atoms, tapered waveguides, and larger trapped-ion systems provides the natural setup to discern between the CE and the local features, as our calculations suggest.

ACKNOWLEDGMENTS

We thank A. Buyskikh and J. C. Halimeh for fruitful discussions. This research was supported by the European Commission FET-Proactive QUIC (H2020 Grant No. 641122) and the Deutsche Forschungsgemeinschaft (DFG) through SFB/CRC1073 (Projects No. B03 and No. C03).

APPENDIX A: BOSE-HUBBARD MODEL

The Bose-Hubbard (BH) model,

$$\hat{H} = -J \sum_{(\mathbf{R}, \mathbf{R}')} (\hat{a}_{\mathbf{R}}^\dagger \hat{a}_{\mathbf{R}'} + \text{H.c.}) + \frac{U}{2} \sum_{\mathbf{R}} \hat{n}_{\mathbf{R}} (\hat{n}_{\mathbf{R}} - 1), \quad (\text{A1})$$

is constructed using the particle operators $\hat{K}_1(\mathbf{R}) \equiv \hat{n}_{\mathbf{R}} (\hat{n}_{\mathbf{R}} - 1)$ and $\hat{K}_2(\mathbf{R}, \mathbf{R}') \equiv -\hat{a}_{\mathbf{R}}^\dagger \hat{a}_{\mathbf{R}'} - \hat{a}_{\mathbf{R}'}^\dagger \hat{a}_{\mathbf{R}}$, where $\hat{a}_{\mathbf{R}}$ and $\hat{n}_{\mathbf{R}} = \hat{a}_{\mathbf{R}}^\dagger \hat{a}_{\mathbf{R}}$ are, respectively, the annihilation and number operators on the lattice site \mathbf{R} . The amplitudes are, respectively, the two-body interaction strength, $h(\mathbf{R}) = U/2$, and the tunnel amplitude $J(\mathbf{R}, \mathbf{R}') = J$. The Bose-Hubbard model has two phases, namely, the superfluid phase for $J \gg U$ and the Mott-insulator phase for $J \ll U$. The precise critical point depends on the dimension and on the average number of particles per site. For a review, see, for instance, Ref. [54].

1. Superfluid phase

In the superfluid phase and for high-enough average particle density in one dimension, $n \gg U/2J$, we may rely on the Bogoliubov mean-field approximation. Assuming small density fluctuations, $\Delta n \ll n$, one develops the interaction term in Eq. (A1) up to quadratic order. The resulting quadratic form is then diagonalized using standard Bogoliubov transformation

(see, for instance, Refs. [16,44]). It yields the gapless dispersion relation

$$E_k \simeq 2\sqrt{2J \sin^2(k/2)[2J \sin^2(k/2) + nU]}. \quad (\text{A2})$$

It is phononic in the low-energy limit, $E_k \simeq ck$, with the sound velocity $c = \sqrt{2nJU}$. At higher energy, it shows an inflection point at some finite momentum $0 < k^* < \pi$, corresponding to the maximum group velocity $V_g^* = V_g(k^*)$.

After the quench, the connected one-body correlation function, $G(R,t) = \langle \hat{a}_R^\dagger(t)\hat{a}_0(t) \rangle - \langle \hat{a}_R^\dagger(0)\hat{a}_0(0) \rangle$, considered in the main text, is then cast into the form of Eq. (2) by mapping the particle operators onto Bogoliubov quasiparticle operators. It yields the amplitude function

$$\mathcal{F}(k) = \frac{2n^2 J U_f (U_f - U_i)}{E_{k,i} E_{k,f}^2} \sin^2(k/2), \quad (\text{A3})$$

where the indices i and f refer to the prequench and postquench values, respectively.

2. Mott insulator phase

In the Mott insulator phase, the model develops a finite gap. The energy excitations may be found using strong-coupling expansions (see, for instance, Refs. [6,55,56]). For $n \in \mathbb{N}^*$ and $U \gg Jn$, it yields low-energy excitations made of doublon-holon pairs of energy,

$$2E_k \simeq U - 2(2n + 1)J \cos(k). \quad (\text{A4})$$

The maximum of the group velocity is at the center of the band, $k^* = \pi/2$, where the group and phase velocities are $V_g^* = (2n + 1)J$ and $V_\varphi^* = U/\pi$, respectively. Hence, for $U > \pi(2n + 1)J$, the phase velocity exceeds the group velocity, $V_\varphi^* > V_g^*$. Note that this regime is well inside the Mott regime where Eq. (A4) is accurate.

Like for the superfluid phase, the connected one-body correlation function can be cast into the form of Eq. (2) with the amplitude function

$$\mathcal{F}(k) = \frac{4Jn(n + 1)}{iU} \sin(k) \quad (\text{A5})$$

for the quench from $U_i = \infty$ to $U_f = U$, as considered in the main text.

APPENDIX B: LONG-RANGE XY AND XXZ MODELS

For spin models, the operators \hat{K}_j represent spin operators, the parameter $J(\mathbf{R}, \mathbf{R}')$ is the exchange term, and $h(\mathbf{R})$ is a magnetic field. For the long-range XY (LRXY) model, we use $\hat{K}_2(\mathbf{R}, \mathbf{R}') \equiv \hat{S}_\mathbf{R}^x \cdot \hat{S}_{\mathbf{R}'}^x + \hat{S}_\mathbf{R}^y \cdot \hat{S}_{\mathbf{R}'}^y$, $J(\mathbf{R}, \mathbf{R}') = -J/2|\mathbf{R} - \mathbf{R}'|^\alpha$, and $h(\mathbf{R}) = 0$. For the initial state, it is generalized to the XXZ model by including an antiferromagnetic exchange coupling in the z direction, which yields the Hamiltonian

$$\hat{H} = \sum_{\mathbf{R} \neq \mathbf{R}'} \frac{J/2}{|\mathbf{R} - \mathbf{R}'|^\alpha} [-(\hat{S}_\mathbf{R}^x \hat{S}_{\mathbf{R}'}^x + \hat{S}_\mathbf{R}^y \hat{S}_{\mathbf{R}'}^y) + \epsilon \hat{S}_\mathbf{R}^z \hat{S}_{\mathbf{R}'}^z]. \quad (\text{B1})$$

For the LRXY case considered in the main text, the quench is performed from the ground state of the XXZ model ($\epsilon \neq 0$) to the XY model ($\epsilon = 0$).

We study the phase where the rotational symmetry around the z axis is spontaneously broken and the spins are polarized

along the x axis. There, the Hamiltonian can be diagonalized using standard Holstein-Primakoff transformation [57,58],

$$\begin{aligned} S_\mathbf{R}^x &= \frac{1}{2} - \hat{a}_\mathbf{R}^\dagger a_\mathbf{R}, \\ S_\mathbf{R}^y &\simeq -\frac{\hat{a}_\mathbf{R}^\dagger - \hat{a}_\mathbf{R}}{2i}, \\ S_\mathbf{R}^z &\simeq -\frac{\hat{a}_\mathbf{R} + \hat{a}_\mathbf{R}^\dagger}{2}, \end{aligned}$$

where terms beyond second order in the boson operators $\hat{a}_\mathbf{R}$ and $\hat{a}_\mathbf{R}^\dagger$ are neglected. Inserting these transformations into Eq. (B1) yields a quadratic Bose Hamiltonian, which can be diagonalized using canonical Bogoliubov transformations (see, for instance, Ref. [51]). For $\epsilon = 0$ (LRXY model), it yields the dispersion relation for $D = 1$,

$$E_k = \frac{J P_\alpha(0)}{2} \sqrt{1 - \frac{P_\alpha(k)}{P_\alpha(0)}}, \quad (\text{B2})$$

where $P_\alpha(k) = \int dR e^{-ik \cdot R} / |R|^\alpha$ is the Fourier transform of the long-range term. In the infrared limit, it can be written

$$P_\alpha(k) \approx P_\alpha(0) + P'_\alpha k^{\alpha-D}, \quad (\text{B3})$$

where $P_\alpha(0)$ and P'_α are finite constants. Hence, we find $E_k \propto |k|^z$ with $z = (\alpha - D)/2$. For $D < \alpha < D + 2$, the quasiparticle energy is finite, but the group velocity V_g diverges in the infrared limit $k \rightarrow 0$.

The connected spin-spin correlation function along the z direction for a quench from $\epsilon_i \neq 0$ to $\epsilon_f = 0$, $G_0(R,t) = \langle S_\mathbf{R}^z(t) S_0^z(t) \rangle - \langle S_\mathbf{R}^z(t) \rangle \langle S_0^z(t) \rangle$, used in the main text, is cast into the form of Eq. (2) using the quasiparticle amplitudes, which yields

$$\mathcal{F}(k) = \frac{\epsilon_i P_\alpha(k)}{8 P_\alpha(0)} \sqrt{\frac{P_\alpha(0) - P_\alpha(k)}{P_\alpha(0) + \epsilon_i P_\alpha(k)}}. \quad (\text{B4})$$

In the infrared limit, it scales as $\mathcal{F}(k) \sim k^\nu$, with $\nu = (\alpha - D)/2 = z$.

The linearization of the Holstein-Primakoff transformation holds for $|1/2 - S_\mathbf{R}^x| \ll 1$ (see Ref. [58]). For the calculations corresponding to Fig. 2 (a), we find $\max\{|1/2 - S_\mathbf{R}^x|\} \simeq 0.12$. It validates the spin-wave approximation used in the main text. This result agrees with the predictions for the same model made in Ref. [51], where the validity of the spin-wave approach for that model was extensively studied.

APPENDIX C: LONG-RANGE TRANSVERSE ISING MODEL

The long-range transverse Ising (LRTI) model corresponds to the spin operators $\hat{K}_1(\mathbf{R}) \equiv \hat{S}_\mathbf{R}^z$ and $\hat{K}_2(\mathbf{R}, \mathbf{R}') \equiv \hat{S}_\mathbf{R}^x \cdot \hat{S}_{\mathbf{R}'}^x$ with a uniform magnetic field $h(\mathbf{R}) = -2h$ and the algebraically decaying exchange amplitude $J(\mathbf{R}, \mathbf{R}') = 2J/|\mathbf{R} - \mathbf{R}'|^\alpha$, which yields

$$\hat{H} = \sum_{\mathbf{R} \neq \mathbf{R}'} \frac{2J}{|\mathbf{R} - \mathbf{R}'|^\alpha} \hat{S}_\mathbf{R}^x \hat{S}_{\mathbf{R}'}^x - 2h \sum_{\mathbf{R}} \hat{S}_\mathbf{R}^z. \quad (\text{C1})$$

The LRTI has two phases [59]. In the z -polarized phase, the dispersion relation can be found using again the

Holstein-Primakoff transformation,

$$\begin{aligned} S_{\mathbf{R}}^x &\simeq \frac{\hat{a}_{\mathbf{R}} + \hat{a}_{\mathbf{R}}^\dagger}{2}, \\ S_{\mathbf{R}}^y &\simeq -\frac{\hat{a}_{\mathbf{R}}^\dagger - \hat{a}_{\mathbf{R}}}{2i}, \\ S_{\mathbf{R}}^z &= \frac{1}{2} - \hat{a}_{\mathbf{R}}^\dagger \hat{a}_{\mathbf{R}}. \end{aligned}$$

One then finds the dispersion relation for $D = 1$,

$$E_k = 2\sqrt{h[h + JP_\alpha(k)]}. \quad (\text{C2})$$

In the infrared limit, where Eq. (B3) holds, it can be expressed as

$$E_k = \Delta + c|k|^z, \quad (\text{C3})$$

where the gap $\Delta = 2\sqrt{h[h + JP_\alpha(0)]}$ is finite, $c = \sqrt{\frac{h}{h + JP_\alpha(0)}}JP'_\alpha$, and $z = \alpha - D$; see Ref. [17]. Hence, the quasiparticle energy is finite, and the group velocity diverges for $D < \alpha < D + 1$.

In the main text, we consider the connected spin-spin correlation function along the x direction, $G_0(R, t) = \langle S_R^x(t)S_0^x(t) \rangle - \langle S_R^x(t) \rangle \langle S_0^x(t) \rangle$, which can be written in the form of Eq. (2) with

$$\mathcal{F}(k) = \frac{h(J_i - J_f)P_\alpha(k)}{8[h + J_f P_\alpha(k)]\sqrt{h[h + J_i P_\alpha(k)]}}. \quad (\text{C4})$$

In the infrared limit, it converges to a finite value. Hence, $\mathcal{F}(k) \sim k^\nu$, with $\nu = 0$.

For the calculations corresponding to the Ising model in Fig. 2(b), we find $\max\{|1/2 - S_{\mathbf{R}}^z|\} = 0.11$, which validates the spin-wave approximation in this case.

APPENDIX D: NUMERICAL ANALYSIS OF THE LOCAL EXTREMA AND THE CORRELATION EDGE FOR THE LRXY AND LRTI MODELS

In the main text, it was shown that the causality cone features a double structure: an outer structure, which determines the correlation edge (CE), and an inner structure, where local extrema propagate. Here we provide details on the numerical analysis of the CE and of the trajectory for the first local extremum for both the LRXY and LRTI models considered in the main text.

1. LRXY model

For the LRXY model, we consider the time evolution of the connected spin-spin correlation function $G(R, t)$ along the z axis. Figure 3 shows the same data as Fig. 2(a) in the main text. To find the CE, we proceed as follows. For each distance R , we trace the activation time $t^*(R)$ corresponding to the first time when a fraction (2%) of the absolute maximum of the correlation function is reached. It yields the solid blue points in Fig. 3. They feature a linear trajectory in the log-log scale, that is, a power-law behavior in linear-linear (lin-lin) scale. The latter is in excellent agreement with the theoretical prediction $\beta_{\text{CE}} \simeq 1.15$, shown as a solid green line. We have also fitted a power-law function, $t^* \propto R^{\beta_{\text{CE}}^{\text{fit}}}$, to the blue points for

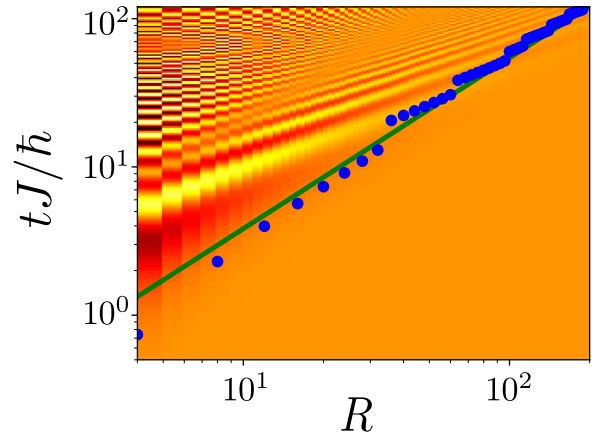


FIG. 3. Spreading of the connected spin-spin correlation function for the LRXY model with $\alpha = 2.3$ [same data as in Fig. 2(a) of the main text; log-log scale]. The solid blue points correspond for each distance R to the first time where the correlation reaches 2% of its maximum value. The solid green line shows the power law predicted theoretically with a fitted multiplicative factor.

$20 < R < 175$ (not shown). It yields $\beta_{\text{CE}}^{\text{fit}} = 1.083 \pm 0.013$, in good agreement with the prediction.

A similar result is obtained on a length scale closer to the one accessible in state-of-the-art experiments [60]. Fitting the same algebraic function to the correlation edge in the range $10 < R < 30$ and $t < 10/J$ yields $\beta_{\text{CE}}^{\text{fit}} = 1.121 \pm 0.012$. It is already in good agreement with the fit in the larger range and with the theoretical prediction.

To analyze the behavior of the local extrema, we trace them from the data of Fig. 3, where they are clearly visible. The result for the first one is plotted in Fig. 4 (solid red line) together with a fitted power law, $t_m = aR^{\beta_m^{\text{fit}}} + b$ (dashed blue line). The fit yields $\beta_m^{\text{fit}} = 0.634 \pm 0.014$, in excellent agreement with the theoretical exponent $\beta_m = 0.65$.

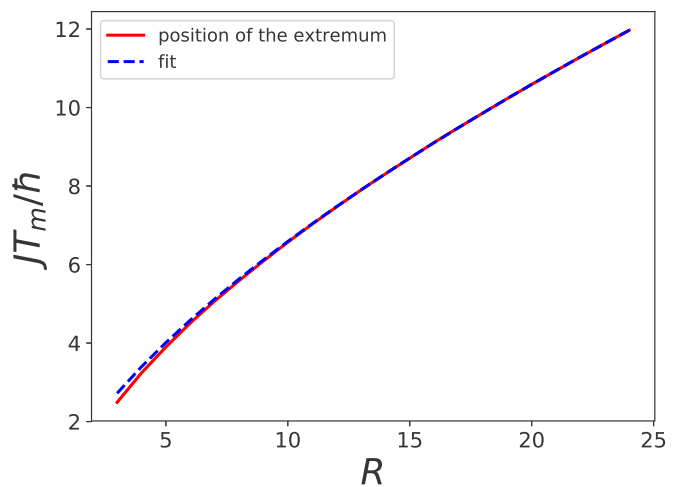


FIG. 4. Trajectory of the first extremum of the connected spin-spin correlation function for the LRXY model (lin-lin scale). The numerical results found from Fig. 3 (solid red line) are shown together with a fitted power law (dashed blue line).

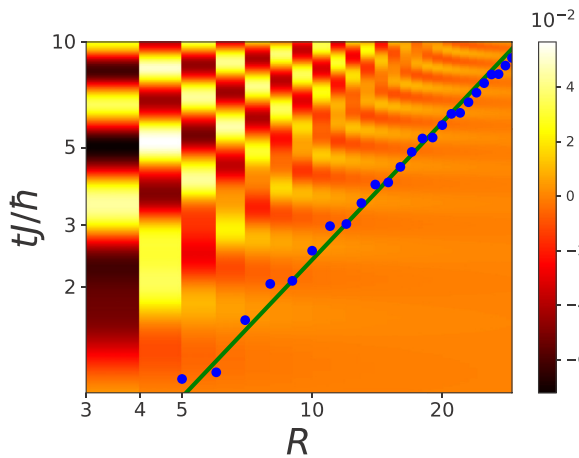


FIG. 5. Spreading of the connected spin-spin correlation function for the LRTI model with $\alpha = 1.7$ [same data as in Fig. 2(b) of the main text; log-log scale]. The solid blue points correspond for each distance R to the first time where the correlation reaches 2.8% of its maximum value. The solid green line shows the power law predicted theoretically with a fitted multiplicative factor.

2. LRTI model

We now turn to the LRTI model and perform the same analysis as above, up to details that we discuss below. Figure 5 shows the same data as Fig. 2(b) in the main text but on a smaller timescale. The CE, corresponding to the trajectory of the first points where the correlation function reaches a fraction (2.8%) of its maximum (solid blue points), matches very well the theoretical prediction $t^* \propto R^{\beta_{\text{CE}}}$, with $\beta_{\text{CE}} = 1.3$ (solid green line with a fitted multiplicative factor). Moreover, fitting a power-law function to the blue points for $4 < R < 30$ yields $\beta_{\text{CE}}^{\text{fit}} = 1.28 \pm 0.02$ (not shown), in perfect agreement with our prediction.

We analyze the trajectory of the maxima in the same way as before. For the LRTI model, ballistic spreading is expected for sufficiently large values of t and R . This is confirmed by the behavior of the local maxima in Fig. 2(b) of the main text.

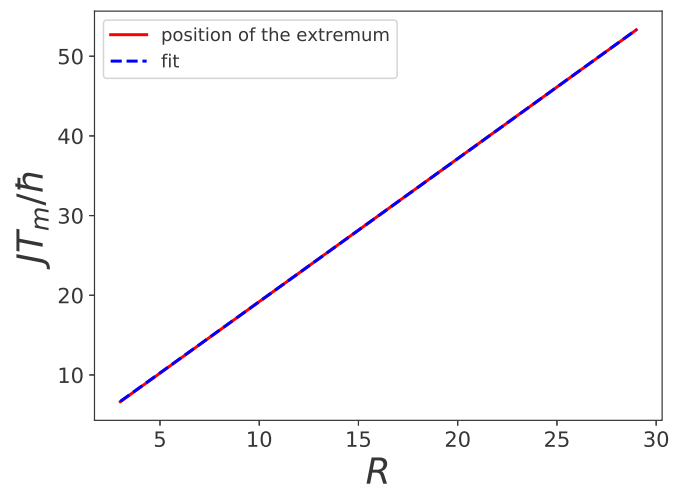


FIG. 6. Trajectory of an extremum of the connected spin-spin correlation function for the LRTI model (lin-lin scale). It corresponds to the dashed dark blue line in Fig. 2(b) of the main text. The numerical results found from Fig. 5 (solid red line) are shown together with a fitted power law (dashed blue line).

The first local maxima are marked by dashed light blue curves. In Fig. 2(b), they are curved owing to the competition between the different terms of the phase of the cosine in Eq. (5). They, however, clearly converge to a ballistic behavior when t and R increase. For the range of t and R presented in Fig. 2(b) the dark blue line is purely ballistic even for small values of t and R . Its trajectory is shown in lin-lin scale in Fig. 6. To confirm the ballistic behavior, we fitted the power-law function $t_m = aR^{\beta_m^{\text{fit}}} + b$ to the data (dashed blue line). The fit gives $\beta_m^{\text{fit}} = 1.0045 \pm 0.0003$, in excellent agreement with the theoretical exponent $\beta_m = 1$.

We have also performed similar fits for the other local maxima, which confirms the asymptotic ballistic behavior. For instance, for the first local maximum [lowest dashed light blue lines in Fig. 2(b)] and $10 < R < 20$, we find $\beta_m^{\text{fit}} = 1.0039 \pm 0.0002$, which is also in excellent agreement with the theoretical prediction.

-
- [1] E. H. Lieb and D. W. Robinson, The finite group velocity of quantum spin systems, *Commun. Math. Phys.* **28**, 251 (1972).
 - [2] S. Bravyi, M. B. Hastings, and F. Verstraete, Lieb-Robinson Bounds and the Generation of Correlations and Topological Quantum Order, *Phys. Rev. Lett.* **97**, 050401 (2006).
 - [3] M. Cheneau, P. Barmettler, D. Poletti, M. Endres, P. Schauss, T. Fukuhara, C. Gross, I. Bloch, C. Kollath, and S. Kuhr, Light-cone-like spreading of correlations in a quantum many-body system, *Nature (London)* **481**, 484 (2012).
 - [4] T. Fukuhara, P. Schausz, M. Endres, S. Hild, M. Cheneau, I. Bloch, and C. Gross, Microscopic observation of magnon bound states and their dynamics, *Nature (London)* **502**, 76 (2013).
 - [5] S. R. Manmana, S. Wessel, R. M. Noack, and A. Muramatsu, Time evolution of correlations in strongly interacting fermions after a quantum quench, *Phys. Rev. B* **79**, 155104 (2009).
 - [6] P. Barmettler, D. Poletti, M. Cheneau, and C. Kollath, Propagation front of correlations in an interacting Bose gas, *Phys. Rev. A* **85**, 053625 (2012).
 - [7] G. Carleo, F. Becca, L. Sanchez-Palencia, S. Sorella, and M. Fabrizio, Light-cone effect and supersonic correlations in one- and two-dimensional bosonic superfluids, *Phys. Rev. A* **89**, 031602(R) (2014).
 - [8] L. Dell'Anna, O. Salberger, L. Barbiero, A. Trombettoni, and V. E. Korepin, Violation of cluster decomposition and absence of light cones in local integer and half-integer spin chains, *Phys. Rev. B* **94**, 155140 (2016).
 - [9] M. Kormos, M. Collura, G. Takacs, and P. Calabrese, Real-time confinement following a quantum quench to a non-integrable model, *Nat. Phys.* **13**, 246 (2017).
 - [10] M. B. Hastings, and T. Koma, Spectral gap and exponential decay of correlations, *Commun. Math. Phys.* **265**, 781 (2006).

- [11] M. Foss-Feig, Z.-X. Gong, C. W. Clark, and A. V. Gorshkov, Nearly Linear Light Cones in Long-Range Interacting Quantum Systems, *Phys. Rev. Lett.* **114**, 157201 (2015).
- [12] P. Hauke and L. Tagliacozzo, Spread of Correlations in Long-Range Interacting Quantum Systems, *Phys. Rev. Lett.* **111**, 207202 (2013).
- [13] J. Eisert, M. van den Worm, S. R. Manmana, and M. Kastner, Breakdown of Quasilocality in Long-Range Quantum Lattice Models, *Phys. Rev. Lett.* **111**, 260401 (2013).
- [14] P. Jurcevic, B. P. Lanyon, P. Hauke, C. Hempel, P. Zoller, R. Blatt, and C. F. Roos, Quasiparticle engineering and entanglement propagation in a quantum many-body system, *Nature (London)* **511**, 202 (2014).
- [15] P. Richerme, Z.-X. Gong, A. Lee, C. Senko, J. Smith, M. Foss-Feig, S. Michalakakis, A. V. Gorshkov, and C. Monroe, Non-local propagation of correlations in quantum systems with long-range interactions, *Nature (London)* **511**, 198 (2014).
- [16] L. Cevolani, G. Carleo, and L. Sanchez-Palencia, Protected quasi-locality in quantum systems with long-range interactions, *Phys. Rev. A* **92**, 041603(R) (2015).
- [17] L. Cevolani, G. Carleo, and L. Sanchez-Palencia, Spreading of correlations in exactly solvable quantum models with long-range interactions in arbitrary dimensions, *New J. Phys.* **18**, 093002 (2016).
- [18] A. S. Buyskikh, M. Fagotti, J. Schachenmayer, F. Essler, and A. J. Daley, Entanglement growth and correlation spreading with variable-range interactions in spin and fermionic tunneling models, *Phys. Rev. A* **93**, 053620 (2016).
- [19] J. Schachenmayer, A. Pikovski, and A. M. Rey, Dynamics of correlations in two-dimensional quantum spin models with long-range interactions: A phase-space Monte-Carlo study, *New J. Phys.* **17**, 065009 (2015).
- [20] J. Schachenmayer, B. P. Lanyon, C. F. Roos, and A. J. Daley, Entanglement Growth in Quench Dynamics with Variable Range Interactions, *Phys. Rev. X* **3**, 031015 (2013).
- [21] M. Kastner, Entanglement-enhanced spreading of correlations, *New J. Phys.* **17**, 123024 (2015).
- [22] V. Bendkowsky, B. Butscher, J. Nipper, J. P. Shaffer, R. Löw, and T. Pfau, Observation of ultralong-range Rydberg molecules, *Nature (London)* **458**, 1005 (2009).
- [23] H. Weimer, M. Müller, I. Lesanovsky, P. Zoller, and H. P. Büchler, A Rydberg quantum simulator, *Nat. Phys.* **6**, 382 (2010).
- [24] P. Schausz, M. Cheneau, M. Endres, T. Fukuhara, S. Hild, A. Omran, T. Pohl, C. Gross, S. Kuhr, and I. Bloch, Observation of spatially ordered structures in a two-dimensional Rydberg gas, *Nature (London)* **491**, 87 (2012).
- [25] A. Browaeys, D. Barredo, and T. Lahaye, Experimental investigations of dipole-dipole interactions between a few Rydberg atoms, *J. Phys. B* **49**, 152001 (2016).
- [26] O. Firstenberg, T. Peyronel, Q.-Y. Liang, A. V. Gorshkov, M. D. Lukin, and V. Vuletic, Attractive photons in a quantum nonlinear medium, *Nat. Phys.* **502**, 71 (2013).
- [27] A. Micheli, G. K. Brennen, and P. Zoller, A toolbox for lattice-spin models with polar molecules, *Nat. Phys.* **2**, 341 (2006).
- [28] B. Yan, S. A. Moses, B. Gadway, J. P. Covey, K. R. A. Hazzard, A. M. Rey, D. S. Jin, and J. Ye, Observation of dipolar spin-exchange interactions with lattice-confined polar molecules, *Nature (London)* **501**, 521 (2013).
- [29] S. A. Moses, J. P. Covey, M. T. Miecikowski, D. S. Jin, and J. Ye, New frontiers for quantum gases of polar molecules, *Nat. Phys.* **13**, 13 (2017).
- [30] A. Griesmaier, J. Werner, S. Hensler, J. Stuhler, and T. Pfau, Bose-Einstein Condensation of Chromium, *Phys. Rev. Lett.* **94**, 160401 (2005).
- [31] Q. Beaufils, R. Chicireanu, T. Zanon, B. Laburthe-Tolra, E. Maréchal, L. Vernac, J.-C. Keller, and O. Gorceix, All-optical production of chromium Bose-Einstein condensates, *Phys. Rev. A* **77**, 061601 (2008).
- [32] M. Lu, N. Q. Burdick, S. H. Youn, and B. L. Lev, Strongly Dipolar Bose-Einstein Condensate of Dysprosium, *Phys. Rev. Lett.* **107**, 190401 (2011).
- [33] S. Baier, M. J. Mark, D. Petter, K. Aikawa, L. Chomaz, Z. Cai, M. Baranov, P. Zoller, and F. Ferlaino, Extended Bose-Hubbard models with ultracold magnetic atoms, *Science* **352**, 201 (2016).
- [34] T. Lahaye, C. Menotti, L. Santos, M. Lewenstein, and T. Pfau, The physics of dipolar bosonic quantum gases, *Rep. Prog. Phys.* **72**, 126401 (2009).
- [35] A. A. Houck, H. E. Tureci, and J. Koch, On-chip quantum simulation with superconducting circuits, *Nat. Phys.* **8**, 292 (2012).
- [36] X.-L. Deng, D. Porras, and J. I. Cirac, Effective spin quantum phases in systems of trapped ions, *Phys. Rev. A* **72**, 063407 (2005).
- [37] R. Islam, E. Edwards, K. Kim, S. Korenblit, C. Noh, H. Carmichael, G.-D. Lin, L.-M. Duan, C.-C. J. Wang, J. Freericks *et al.*, Onset of a quantum phase transition with a trapped ion quantum simulator, *Nat. Commun.* **2**, 377 (2011).
- [38] B. P. Lanyon, C. Hempel, D. Nigg, M. Müller, R. Gerritsma, F. Zähringer, P. Schindler, J. T. Barreiro, M. Rambach, G. Kirchmair *et al.*, Universal digital quantum simulation with trapped ions, *Science* **334**, 57 (2011).
- [39] C. Schneider, D. Porras, and T. Schaetz, Experimental quantum simulations of many-body physics with trapped ions, *Rep. Prog. Phys.* **75**, 024401 (2012).
- [40] R. Blatt and C. F. Roos, Quantum simulations with trapped ions, *Nat. Phys.* **8**, 277 (2012).
- [41] L. Childress, M. V. Gurudev Dutt, J. M. Taylor, A. S. Zibrov, F. Jelezko, J. Wrachtrup, P. R. Hemmer, and M. D. Lukin, Coherent dynamics of coupled electron and nuclear spin qubits in diamond, *Science* **314**, 281 (2006).
- [42] G. Balasubramanian, P. Neumann, D. Twitchen, M. Markham, R. Kolesov, N. Mizuochi, J. Isoya, J. Achard, J. Beck, J. Tissler *et al.*, Ultralong spin coherence time in isotopically engineered diamond, *Nat. Mater.* **8**, 383 (2009).
- [43] F. Dolde, I. Jakobi, B. Naydenov, N. Zhao, S. Pezzagna, C. Trautmann, J. Meijer, P. Neumann, F. Jelezko, and J. Wrachtrup, Room-temperature entanglement between single defect spins in diamond, *Nat. Phys.* **9**, 139 (2013).
- [44] S. S. Natu and E. J. Mueller, Dynamics of correlations in a dilute Bose gas following an interaction quench, *Phys. Rev. A* **87**, 053607 (2013).
- [45] I. Frérot, P. Naldesi, and T. Roscilde, Multispeed prethermalization in quantum spin models with power-law decaying interactions *Phys. Rev. Lett.* **120**, 050401 (2018).
- [46] J. Haegeman, B. Pirvu, D. J. Weir, J. I. Cirac, T. J. Osborne, H. Verschelde, and F. Verstraete, Variational matrix product ansatz for dispersion relations, *Phys. Rev. B* **85**, 100408 (2012).

- [47] N. Nakatani, S. Wouters, D. V. Neck, and G. K.-L. Chan, Linear response theory for the density matrix renormalization group: Efficient algorithms for strongly correlated excited states, *J. Chem. Phys.* **140**, 024108 (2014).
- [48] For simplicity, we assume that, if it exists, there is a single solution \mathbf{k}_{sp} . Should Eq. (3) have several solutions, Eq. (4) is replaced by the sum of the corresponding contributions [16].
- [49] P. Calabrese and J. Cardy, Time Dependence of Correlation Functions Following a Quantum Quench, *Phys. Rev. Lett.* **96**, 136801 (2006).
- [50] No clear double structure is visible in Fig. 1(a) of Ref. [7] because it corresponds to $Un = 4$, where the group and phase velocities are almost equal.
- [51] I. Frérot, P. Naldesi, and T. Roscilde, Entanglement and fluctuations in the XXZ model with power-law interactions, *Phys. Rev. B* **95**, 245111 (2017).
- [52] For the LRTI model with $\alpha = 1.7$, the phase transition between the polarized and Néel phases is located around $J/h \simeq 3$; see Ref. [59].
- [53] The dependence on D and ν completely disappears in the limit of a spectrum with a nondivergent velocity, $z \rightarrow 1^-$, in agreement with the general LR picture [1].
- [54] A. Georges and T. Giamarchi, Strongly correlated bosons and fermions in optical lattices, in *Many-Body Physics with Ultracold Gases*, edited by C. Salomon, G. V. Shlyapnikov, and L. F. Cugliandolo, Proceedings of the Les Houches Summer School of Theoretical Physics Vol. 94 (Oxford University Press, Oxford, 2012), pp. 1–70.
- [55] E. Altman and A. Auerbach, Oscillating Superfluidity of Bosons in Optical Lattices, *Phys. Rev. Lett.* **89**, 250404 (2002).
- [56] S. D. Huber, E. Altman, H. P. Büchler, and G. Blatter, Dynamical properties of ultracold bosons in an optical lattice, *Phys. Rev. B* **75**, 085106 (2007).
- [57] T. Holstein and H. Primakoff, Field dependence of the intrinsic domain magnetization of a ferromagnet, *Phys. Rev.* **58**, 1098 (1940).
- [58] A. Auerbach, *Interacting Electrons and Quantum Magnetism* (Springer, New York, 1994).
- [59] T. Koffel, M. Lewenstein, and L. Tagliacozzo, Entanglement Entropy for the Long-Range Ising Chain in a Transverse Field, *Phys. Rev. Lett.* **109**, 267203 (2012).
- [60] J. Zhang, G. Pagano, P. W. Hess, A. Kyprianidis, P. Becker, H. Kaplan, A. V. Gorshkov, Z.-X. Gong, and C. Monroe, Observation of a many-body dynamical phase transition with a 53-qubit quantum simulator, *Nature (London)* **551**, 601 (2017).